Engineering xxx (xxxx) xxx

Contents lists available at ScienceDirect

Engineering

journal homepage: www.elsevier.com/locate/eng

Research
Microecology—Article

STAT3-Dependent Effects of Polymeric Immunoglobulin Receptor in Regulating Interleukin-17 Signaling and Preventing Autoimmune Hepatitis

Ting Li [a,b,#], Tongtong Pan [a,#,*], Nannan Zheng [a], Xiong Ma [c], Xiaodong Wang [a], Fang Yan [a], Huimian Jiang [a], Yuxin Wang [a], Hongwei Lin [a], Jing Lin [a], Huadong Zhang [a], Jia Huang [a], Lingming Kong [d], Anmin Huang [d], Qingxiu Liu [e], Yongping Chen [a,*], Dazhi Chen [a,b,*]

[a] *Hepatology Diagnosis and Treatment Center, The First Affiliated Hospital of Wenzhou Medical University & Zhejiang Provincial Key Laboratory for Accurate Diagnosis and Treatment of Chronic Liver Diseases, Wenzhou 325035, China*
[b] *Department of Clinical Medicine, Hangzhou Medical College, Hangzhou 310053, China*
[c] *Division of Gastroenterology and Hepatology, Key Laboratory of Gastroenterology and Hepatology, Ministry of Health, State Key Laboratory for Oncogenes and Related Genes, Renji Hospital, School of Medicine, Shanghai Jiao Tong University, Shanghai 200001, China*
[d] *Wenzhou Medical University, Wenzhou 325035, China*
[e] *Division of Infectious Diseases, Lishui People's Hospital, Lishui 323000, China*

ARTICLE INFO

Article history:
Received 14 July 2023
Revised 29 December 2023
Accepted 1 January 2024
Available online 20 January 2024

Keywords:
Autoimmune hepatitis
Polymeric immunoglobulin receptor
Regenerating islet-derived 3 beta
Intestinal microbiota
Signal transducer and activator of transcription 3

ABSTRACT

One-third of patients with autoimmune hepatitis (AIH) have cirrhosis at the time of diagnosis. The relevance of these variables, although unknown, is believed to be critical in AIH because of suspected interactions between the gut microbiome and genetic factors. Dysbiosis of the gut flora and elevated polymeric immunoglobulin receptor (pIgR) levels have been observed in both patients and mouse models. Moreover, there is a direct relationship between pIgR expression and transaminase levels in patients with AIH. In this study, we aimed to explore how pIgR influences the secretion of regenerating islet-derived 3 beta (Reg3b) and the flora composition in AIH using *in vivo* experiments involving patients with AIH and a concanavalin A-induced mouse model of AIH. Reg3b expression was reduced in pIgR gene (*Pigr*)-knockout mice compared to that in wild-type mice, leading to increased microbiota disruption. Conversely, exogenous pIgR supplementation increased Reg3b expression and maintained microbiota homeostasis. RNA sequencing revealed the participation of the interleukin (IL)-17 signaling pathway in the regulation of Reg3b through pIgR. Furthermore, the introduction of external pIgR could not restore the imbalance in gut microbiota in AIH, and the decrease in Reg3b expression was not apparent following the inhibition of signal transducer and activator of transcription 3 (STAT3). In this study, pIgR facilitated the upregulation of Reg3b via the STAT3 pathway, which plays a crucial role in preserving the balance of the intestinal microbiota in AIH. Through this research, we discovered new molecular targets that can be used for the diagnosis and treatment of AIH.

1. Introduction

Autoimmune hepatitis (AIH) is a long-term liver disease characterized by gradual inflammation of the liver and hepatocyte damage. This disorder is intricate and multifaceted, and arises from the interplay between genetic predispositions, environmental triggers, and the host immune system [1]. An imbalance in the gut microbiota has been suggested as a significant factor in the development of AIH [2,3]. Nevertheless, the precise molecular mechanisms responsible for this condition, specifically the mechanisms underlying the modified microbiota and their influence on AIH, are not fully understood.

Polymeric immunoglobulin receptor (pIgR) covalently binds and stabilizes immunoglobulin A (IgA) and transports dimeric IgA across the epithelium [4]. By incorporating both natural and

* Corresponding authors.
E-mail addresses: ptt_wmu@163.com (T. Pan), cyp@wmu.edu.cn (Y. Chen), dazhichen@126.com (D. Chen).
[#] These authors contributed equally to this work.

https://doi.org/10.1016/j.eng.2024.01.006

Please cite this article as: T. Li, T. Pan, N. Zheng et al., STAT3-Dependent Effects of Polymeric Immunoglobulin Receptor in Regulating Interleukin-17 Signaling and Preventing Autoimmune Hepatitis, Engineering, https://doi.org/10.1016/j.eng.2024.01.006

acquired immunity, mucosal epithelial tissues play a crucial role in regulating the gut microbiota by eliminating excess bacteria and actively choosing beneficial symbionts [5]. Changes in the intestinal chemical barrier, including alterations in lysozymes and certain antimicrobial peptides, have been observed in pIgR gene (*Pigr*)-knockout (KO) mice [6]. Through its conventional function of transporting IgA, our previous studies demonstrated that pIgR plays a vital role in regulating mucosal immunity and sustaining a well-balanced gut microbiome in S100-induced AIH mice [7]. Nevertheless, the effect of pIgR on the manifestation of antimicrobial peptides in AIH remains unclear.

Regenerating islet-derived 3 beta gene (*Reg3b*) belongs to the *Reg* gene family and encodes C-type lectin proteins primarily found in epithelial cells [8]. Regulation of the gut microbiota and provision of antimicrobial effects are crucial functions of Reg3b in host defense [9]. It attaches to carbohydrate components on the outer layer of bacteria, specifically Gram-positive bacteria, and effectively eliminates these microorganisms [10]. The antimicrobial activity of Reg3b helps to maintain intestinal homeostasis.

Signal transducer and activator of transcription 3 (STAT3), a member of the STAT protein family, functions as both a signal transducer and transcriptional activator [11]. This process is activated through phosphorylation at the Tyr705 site, followed by translocation into the nucleus for the regulation of gene transcription. Several studies have demonstrated its significant involvement in the release of antimicrobial peptides of the Reg family and the gut microbiota [12,13].

Therefore, this study aimed to investigate the role of pIgR in the secretion of Reg3b and flora composition in AIH by analyzing fecal samples from patients with AIH and via a mouse model of concanavalin A (ConA)-induced AIH.

2. Materials and methods

Table S1 in Appendix A summarizes the main resources used in this study.

2.1. Patients

Patients diagnosed with AIH were categorized according to clinical guidelines [14]. Individuals who had received hormone therapy, antimicrobials, or beneficial bacterial supplements within the past two months were excluded [15]. All patients (n = 15) and healthy controls (n = 15) provided informed consent, and fecal samples were collected in accordance with the procedures approved by the Ethics Committee in Clinical Research of the First Affiliated Hospital of Wenzhou Medical University (KY-2022-155). The raw data pertaining to human subjects can be accessed from the National Center for Biotechnology Information Sequence Read Archive (NCBI SRA) under the project identifier PRJNA1045518[†]. Clinical information of the patients is shown in Table S2 in Appendix A.

2.2. Mouse treatments

Male wild-type (WT) and *Pigr*-KO mice (C57BL/6, 6–8 weeks old) were maintained in a sterile environment. All animal procedures were approved by the Laboratory Animal Ethics Committee (WYYY-AEC-2021-293). AIH model mice were intravenously injected with ConA at a dosage of 15 or 20 $mg \cdot kg^{-1}$. pIgR-treated mice were intraperitoneally injected with mouse pIgR immediately after ConA injection. Each alternative broad-spectrum antibiotic (Abx)-treated mouse was treated daily with an antibiotic cocktail (1.86 mg of ampicillin sodium, 0.96 mg of vancomycin hydrochloride, 1.86 mg of neomycin sulfate, and 1.20 mg of metronidazole) at a dosage of 0.1 mL by oral gavage for three weeks before ConA injection to eliminate normal gut flora. We disrupted the expression of intestinal *Reg3b* or *Stat3* by injecting approximately 1×10^{11} genomic copies of adeno-associated virus 9 (AAV9)-mouse-*Reg3b* through the tail vein or administering an enema of 1×10^{11} genomic copies of AAV7-mouse-*Stat3*. Mice treated with interleukin (IL)-17D received an intraperitoneal injection of IL-17D at a dosage of 15 $\mu g \cdot kg^{-1}$ immediately after ConA injection. The mice were randomly divided into 32 groups, as detailed in Table S3 in Appendix A.

2.3. Plate fecal colony culture

Mouse feces (200 mg) was dissolved in 1 mL of normal saline at 37 °C. The filtrate was filtered through a 200-mesh sterile mesh screen to remove large particles, passed through 400- and 800-mesh sterile mesh screens to remove undigested food and smaller particulate matter, and collected in sterile centrifuge tubes. After suspension, the samples were centrifuged at 600g (1g = 9.8 $m \cdot s^{-2}$) for 5 min to eliminate any insoluble matter. The resulting solution was coated in Luria–Bertani medium and cultured overnight in an anaerobic incubator at 37 °C.

2.4. Isolation of small intestinal epithelial cells (IECs)

Fat tissue and Peyer's patches were extracted from the small intestines of mice. The intestine was minced into 0.5 cm pieces. Ten milliliters of IEC isolation buffer, consisting of 90.4 % Hanks' balanced salt solution, 1.4% 0.5 $mol \cdot L^{-1}$ ethylenediaminetetraacetic acid, 0.2% pancreatin, 2% 1 $mol \cdot L^{-1}$ 4-(2-hydroxylethyl)-1-piperazineethanesulfonic acid, 1% 0.1 $mol \cdot L^{-1}$ dithiothreitol, and 5% fetal bovine serum (FBS), was added. Digestion was conducted at 200 $r \cdot min^{-1}$ for 15 min. The filtrate was centrifuged at 600g for 10 min at 4 °C. Cell pellets were collected and washed extensively with phosphate-buffered saline (PBS). The 37 °C lamina propria (LP) digestion buffer was added, and digestion was conducted at 37 °C and 200 $r \cdot min^{-1}$ in a shaker for 45 min. The supernatant was centrifuged at 600g, 4 °C for 10 min to collect the cell pellet. The cells were resuspended in 4 mL of 40% Percoll and layered on top of 20% Percoll. Centrifugation was conducted at 800g for 20 min at a temperature of 20 °C. The layer that formed at the interface after centrifugation contained IECs.

2.5. Biochemical analysis and tissue histopathology

Serum was obtained from blood by centrifugation at 1500 $r \cdot min^{-1}$ for 15 min. Aspartate aminotransferase (AST) and alanine aminotransferase (ALT) were determined using an automated chemistry analyzer (Beckman Coulter, USA). Hematoxylin and eosin (H&E) were used to stain tissue sections embedded in paraffin. Images were captured using microscopy (Nikon, Japan).

2.6. Quantitative real-time polymerase chain reaction (qRT-PCR) assay

An isolation kit was used to extract total RNA from feces or tissues. Next, reverse transcription was performed using PrimeScript RT Master Mix (Takara Bio, USA), followed by qRT-PCR using TB Green. The analysis was performed using an 7500 Real-Time PCR System (Applied Biosystems, USA). The messenger RNA (mRNA) levels of each gene were normalized to that of actin beta (*actb*) and adjusted. Primer sequences are listed in Table S4 in Appendix A.

2.7. Western blot (WB) analysis

Proteins from the liver and intestinal tissues were isolated and quantified using a bicinchoninic acid (BCA) kit. Protein samples

[†] https://www.ncbi.nlm.nih.gov/bioproject/PRJNA1045518

were separated on a 12% sodium dodecyl sulfate-polyacrylamide gel electrophoresis gel and subsequently transferred onto membranes. These membranes were probed with primary antibodies, followed by incubation with the corresponding secondary antibodies. Protein bands were visualized by chemiluminescence image analysis.

2.8. Enzyme-linked immunosorbent assay (ELISA)

Proteins were isolated from feces [16]. A BCA kit was used to determine the quantity of available protein. Quantification of Reg3b, pIgR, IL-17D, IL-22, and lipopolysaccharide (LPS) was performed using assay kits provided by the manufacturer.

2.9. Isolation and flow cytometry of LP immune cells

Small intestinal tissue was collected 10 cm distal to the pyloric sphincter. Peyer's patches and adipose tissues were isolated and thoroughly washed, and LP lymphocytes were separated using a mouse LP dissociation kit. The lymphocytes were resuspended in Roswell Park Memorial Institute (RPMI) 1640 medium (with 10% FBS and 1% penicillin/streptomycin) at a concentration of approximately 2×10^6 mL^{-1}. Sterile 24-well plates were prepared, with 1 mL of cell suspension added to each well, followed by the addition of 2 μL Leukocyte Activation Cocktail (BD Biosciences, USA) to stimulate the cells. The plates were incubated for 4 h at 37 °C. Cells were harvested, centrifuged to remove the supernatant, and resuspended in PBS containing 2% bovine serum albumin. Fluorescently-conjugated antibodies for allophycocyanin/cyanine 7-cluster of differentiation 3 (CD3), CD11b, lymphocyte antigen 6 complex locus G6D, CD45, and fluorescein 5 isothiocyanate-natural killer cell p46 were added and incubated at 4 °C, protected from light, for 60 min. The cells were centrifuged to remove the unbound antibodies and washed twice with PBS. The cells were fixed for 15 min using a cell fixation solution, centrifuged, and permeabilized with 0.1% Triton X-100 for 10 min. Peridinin–chlorophyll protein complex/cyanine5.5-retinoic acid receptor-related orphan receptor γT (RORγt) antibody was added and incubated in the dark at 4 °C for 60 min. 2-(4-amidinophenyl)-6-indole carbamidine dihydrochloride (DAPI) was added at a concentration of 0.5 $μg·mL^{-1}$ for nuclear staining and protected from light for 20 min. After two final PBS washes, the cells were resuspended in buffer, filtered, and analyzed by flow cytometry using a BD LSRFortessa instrument (BD Biosciences).

2.10. Analysis of intestinal microbiota

Cetyltrimethylammonium bromide was used to extract DNA from fecal samples. The integrity of the genomic DNA was detected by agarose gel electrophoresis, and the concentration and purity of the genomic DNA were determined using Nanodrop 2000 and Qubit 3.0 spectrophotometers (Thermo Fisher Scientific, USA). The examination concentrated on the amplicon's V4–V5 region [17] with the primers 515F (5′-GTGCCAGCMGCCGCGG-3′) and 907R (5′-CCGTCAATTCMTTTRAGTTT-3′). The PCR products were purified using AMPure XT beads (Beckman Coulter) and quantified using a Qubit 3.0 (Invitrogen, USA). The amplicon library was prepared for sequencing using the Library Quantification Kit (Illumina, USA) and its size was assessed using an Agilent 2100 Bioanalyzer (Agilent Technologies, USA). NovaSeq PE250 (Illumina) was used for sequencing. Raw read sequences were processed using QIIME2[†]. The adaptor and primer sequences were trimmed using the Cutadapt plugin. High-quality tags were obtained by quality filtering using fqtrim (v0.94). Vsearch (v2.3.4) software was used to eliminate chimeras. After de-replication with a high-resolution sample inference from Illumina amplicon data, DADA2, an amplicon sequence variant table and representative sequences were obtained. Taxonomic assignments of amplicon sequence variant representative sequences were performed with a confidence threshold 0.8 by a pre-trained Naive Bayes classifier, which was trained on the Ribosomal Database Project (version 11). Alpha and beta diversity metrics were determined in QIIME2 by normalizing the number of randomly-selected sequences per sample using QIIME2 and were visualized using R packages (R Core Team). The representative sequences were aligned using Basic Local Alignment Search Tool and functionally annotated using the RDP database (version 11).

[†] https://qiime2.org.

2.11. Analysis of intestinal transcriptomic profiling

Total RNA was extracted using a TRIzol reagent kit (Invitrogen). The RNA quality was assessed using an Agilent 2100 bioanalyzer. Oligo (dT) beads were used to enrich eukaryotic mRNA, and the Ribo-ZeroTM Kit (Epicentre, USA) was used for prokaryotic mRNA enrichment. Random primers were used to fragment the mRNA and subsequently reverse-transcribe it into complementary DNA (cDNA). DNA polymerase I, ribonuclease H, and deoxyribonucleoside triphosphates were used to generate second-strand cDNA. For Illumina sequencing, the cDNA fragments were subjected to end repair, addition of poly(A), and ligation of Illumina sequencing adapters. After sorting the ligated products according to their size on agarose gel, they were amplified by PCR and subsequently sequenced using Illumina HiSeq2500. Clean reads were obtained by filtering the sequencing data using FastP (version 0.18.0). The genes were labeled using Ensembl 104. Gene expression was compared between groups using DESeq2 and EdgeR software. Genes or transcripts were identified as differentially expressed if they had a false discovery rate < 0.05.

2.12. Statistical analysis

All statistical analyses were conducted using GraphPad Prism (v9.3.1; GraphPad Software Inc., USA) and R software (v4.1.1; R Core Team 2021). A Student's *t*-test was used to evaluate two groups, while one-way analysis of variance (ANOVA) or two-way ANOVA with Fisher's least significant difference test or Bonferroni test was used to evaluate multiple groups. The Spearman's rank correlation test (two-tailed) was used to examine the association between pIgR, clinical indices, and gut microbes. GraphPad Prism v9.3.1 was utilized to generate histograms and survival curves. Using ImageJ (v.1.51 k; NIH, USA), we assessed the necrotic region of the liver, the dimensions of the villi (length), and determined the crypt size. This technique was also used for WB. Data were presented in all instances as the average ± standard deviation of three separate trials. The levels of statistical significance were $^{*}P < 0.05$, $^{**}P < 0.01$, $^{***}P < 0.001$, and $^{****}P < 0.0001$.

3. Results

3.1. Elevated fecal pIgR levels in patients with AIH and disordered gut microbiota

Individuals diagnosed with AIH exhibit an imbalanced gut microbiota and diminished microbial variety. The decreased diversity in the stool microbiota of patients with AIH, as measured by the Chao1 and Shannon indices (Figs. S1(a) and (b) in Appendix A) likely reflected gut dysbiosis, which contributes to AIH pathogenesis and progression. Fig. S1(c) in Appendix A shows that patients with AIH and healthy controls had significantly different

overall microbial compositions, as revealed by permutational multivariate analysis of variance ($P < 0.001$). As shown in Fig. 1(a) and Fig. S1(d) in Appendix A, the relative abundances of *Bacteroides*, *Prevotella*, *Blautia*, and *Fecalibacterium* increased, whereas the relative abundances of *Akkermansia* and *Lactobacillus* decreased. The findings of this study exhibited patterns comparable to those of previous studies [18–20], indicating that the gut microbiome could serve as a promising target for therapeutic intervention.

Recent research has demonstrated increased expression of pIgR in autoimmune liver disorders, such as primary biliary cirrhosis [21]. However, limited investigations have been conducted on pIgR expression in AIH. PCR and ELISA were used to measure fecal pIgR levels, revealing that individuals with AIH exhibited notably elevated fecal pIgR concentrations compared to the healthy control group (Figs. 1(b) and (c)). To examine the relationship between pIgR expression and disease-associated genera in patients with AIH, a partial Spearman's rank-based correlation test was conducted (Fig. 1(d)). The expression of pIgR correlated with the abundance of 17 taxa at the genus level. For instance, the abundance of the *Enterococcus* and *Bacteroides* genera was positively correlated with pIgR expression, and the abundances of *Barnesiella*, *Akkermansia*, and *Fecalibacterium* exhibited a negative correlation. Fig. 1(e) shows Pearson's correlation analysis results which revealed a positive correlation between pIgR and host factors, including ALT, AST,

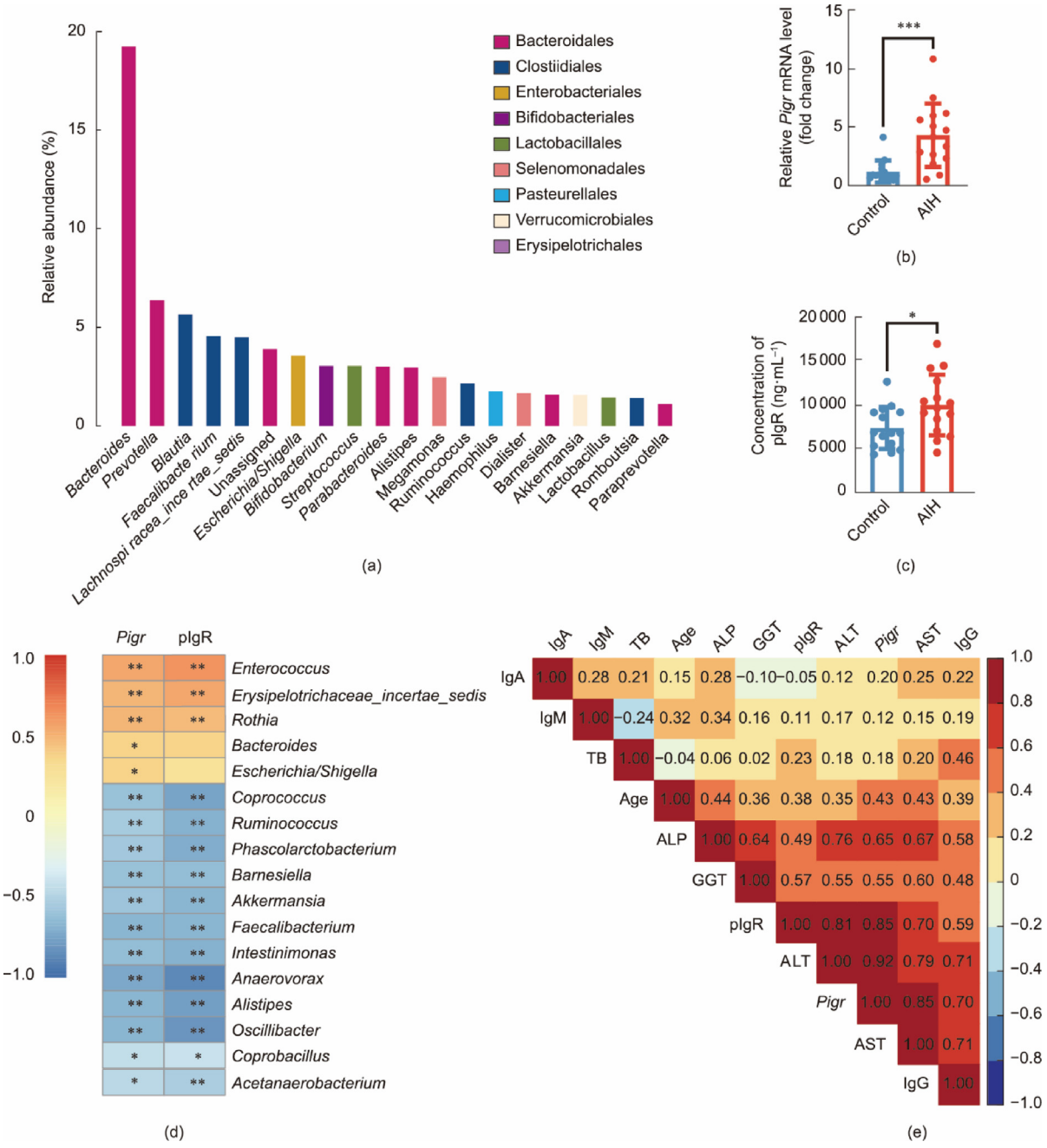

Fig. 1. Disordered gut microbiota and elevated fecal pIgR levels in patients with AIH. (a) Genus-level histogram displaying the overall abundance of species. (b) Comparative analysis of *Pigr* mRNA levels in human fecal samples. ***$P < 0.001$. (c) ELISA for pIgR production in human feces. *$P < 0.05$. (d) Spearman's correlation coefficients between 17 genera and pIgR levels. *$P < 0.05$, **$P < 0.01$. (e) Pearson correlations between pIgR levels and host indexes. $n = 15$ per group. (d, e) unpaired student *t*-test. TB: total bilirubin; ALP: alkaline phosphatase; GGT: gamma-glutamyltransferase.

and IgG, which were used to evaluate the extent of damage caused by AIH.

3.2. Intestinal pIgR is positively correlated with the pathological development of AIH

Following the transcytosis of IgA or IgM mediated by pIgR through intestinal cells, these Igs are released into the intestinal lumen along with pIgR-derived secreted components [22]. Elevated hepatic pIgR levels activate the IgA transport pathway, leading to increased intestinal pIgR [23]. To ascertain whether elevated fecal pIgR expression originated from intestinal or hepatic overexpression, we evaluated pIgR levels in the intestine and liver in a ConA-induced AIH mouse model.

The ConA-induced AIH mouse model showed a clear increase in lymphocyte infiltration surrounding the central vein of the liver lobule, accompanied by a gradual increase in diffuse edema and hepatocyte necrosis (Fig. 2(a)). Serum ALT, AST, and liver necrosis area of mice reached their peak values during 18 h of ConA-induced experimental AIH and then gradually decreased (Figs. 2(a)–(c)). Liver inflammatory markers also changed over time (Table S5 in Appendix A). Subsequently, we discovered that there was no significant alteration in the pIgR level in the liver, whereas the pIgR level in the intestinal tissue exhibited a notable increase as the severity of liver injury increased (Figs. 2(d)–(j)). We hypothesized that the increased presence of intestinal pIgR could potentially account for the elevated levels of pIgR in feces, whereas the abundance of pIgR in gut tissues was linked to the severity of AIH.

3.3. pIgR abrogation significantly accentuates AIH through intestinal flora dysregulation, intestinal villus damage, and decreased Reg3b secretion

To investigate the involvement of pIgR in the advancement and progression of AIH, we established a *Pigr*-KO mouse model and intravenously administered ConA (Fig. 3(a)). The *Pigr*-KO group exhibited poorer overall survival following intravenous administration of ConA at a dose of 20 $mg{\cdot}kg^{-1}$ than the WT group (Fig. 3(b)). Compared with WT mice, *Pigr*-KO mice exhibited a larger liver necrotic area (Fig. 3(c)). After *Pigr* knockout, the ALT and AST levels increased (Figs. 3(d) and (e)). The elevated inflammatory factors, including interleukin genes (*Il1β*, *Il10*, *Il17*), tumor necrosis factor alpha gene (*Tnfα*), transforming growth factor beta gene (*Tgfβ*), and interferon gamma gene (*Ifnγ*) (Figs. S2(a)–(f) in Appendix A) also exhibited significant differences.

In addition, we performed mRNA sequencing of the intestinal tissue while profiling the microbiota in fecal samples, allowing us to explore the relationship between the genotype and the gut microbiome using multiple proteomic approaches. Fig. S2(g) in Appendix A shows intestinal villus degeneration and necrosis in ConA-induced *Pigr*-KO mice. The gut microbiome of *Pigr* deficient mice was dissimilar to that of WT mice (Fig. S2(h) in Appendix A). The knockout of *Pigr* disrupts the equilibrium of the gut microbiome and diminishes the diversity of bacterial species. Fig. S2(i) in Appendix A shows the alterations in the proportions of specific bacterial phyla and genera. For example, the levels of *Escherichia-Shigella*, *Akkermansia*, and *Muribaculum* were enriched in the *Pigr*-KO mice. *Lachno spiraceae_NK4A 136_group*, *Clostridia_UCG−014_unclassified*, *Candidatus_Saccharimonas*, and *Lactobacillus* were decreased. Apart from the biological barrier, mechanical and chemical defenses of the gut make indispensable contributions to preserving intestinal equilibrium [24]. Furthermore, we successfully cleared the intestinal flora with Abx treatment to further analyze the role of the flora in *Pigr*-KO mice (Figs. S3(a) and (b) in Appendix A). Administration of antibiotics reduced ConA-induced liver injury in *Pigr*-KO mice, while exacerbating the injury in WT mice. *Pigr*-KO mice treated with Abx exhibited a reduced necrotic area, lower levels of ALT and AST, and decreased inflammatory cytokines including *Il1β*, *Il17*, *Tnfα*, and *Ifnγ* in comparison to *Pigr*-KO mice without Abx treatment (Figs. S3(c)–(l) in Appendix A). Measurements in WT mice treated with Abx showed contrasting trends. The findings of this study suggest that the augmented vulnerability of *Pigr*-KO mice to AIH can be attributed, at least in part, to intestinal dysbiosis resulting from *Pigr* deficiency.

The expression levels of intestinal barrier-related genes were measured using RNA sequencing (Fig. 3(f)). In *Pigr* deficiency, the expression of occludins and claudins, which are tight junction proteins, remains unchanged, whereas there are noticeable alterations in the expression of certain antimicrobial peptides. In *Pigr*-KO AIH mice, the expression of *Reg3b*, *Ang4*, and *Lyz1* decreased. Among the various antimicrobial peptides examined, *Reg3b* exhibited the most substantial increase in expression (Fig. S3(m) in Appendix A), suggesting a significant contribution to the host defense response. Simultaneously, the levels of Reg3b were elevated in the fecal samples of patients with AIH (Fig. S3(n) in Appendix A), further underscoring its potential relevance in disease pathology. Additional analyses were performed to determine Reg3b protein and mRNA levels in *Pigr*-KO mice. As shown in Figs. 3(g) and (h), the decreased alterations in Reg3b protein levels were the same as the alterations in *Reg3b* mRNA levels in intestinal tissues after *Pigr* knockout.

In summary, *Pigr* knockout led to severe liver and intestinal necrosis, gut microbiota dysbiosis, and reduced Reg3b secretion. These findings collectively demonstrate that pIgR plays a crucial role in preserving tissue integrity and the balance of microbiota, potentially by controlling antimicrobial peptides such as Reg3b. The dysfunction of these functions due to *Pigr* deficiency might be responsible for the pathological phenotypes observed in this investigation.

3.4. Exogenous pIgR protein ameliorates liver injury and intestinal dysbiosis in ConA-induced mice

Worsened liver injury, disturbance of gut microbiota, and dysregulated Reg3b secretion observed in *Pigr*-KO mice indicate the potential protective and homeostatic functions of pIgR against AIH. To elucidate the underlying mechanism, we administered exogenous pIgR to mice with ConA-induced hepatitis (Fig. 4(a)). The doses used were 50, 100, and 200 $mg{\cdot}kg^{-1}$. Low-dose (50 $mg{\cdot}kg^{-1}$) pIgR treatment did not significantly alleviate ConA-induced liver injury. The reduction in the liver necrotic area (Figs. 4(b) and (c)) and alleviation of elevated serum ALT and AST levels (Figs. 4(d) and (e)) were not statistically significant. However, a clear therapeutic effect against ConA-induced hepatitis was observed with increasing pIgR doses. The area of liver necrosis was significantly reduced (Figs. 4(b) and (c)), suggesting mitigation of hepatocyte death and decreased inflammatory infiltration. Similarly, the serum ALT and AST levels, which indicate the degree of liver injury, were significantly decreased (Figs. 4(d) and (e)). Simultaneously, there was a noticeable decrease in the production of pro-inflammatory cytokines such as *Ifnγ*, *Tnfα*, *Il17*, and *Il1β*; conversely, there was an increase in the secretion of anti-inflammatory substances such as *Il10* and *Tgfβ* was prominently upregulated (Figs. S4(a)–(f) in Appendix A). Collectively, these data show that pIgR has varying degrees of protective effects on the liver against immune-mediated injury caused by ConA. This may be achieved by regulating the cytokine environment to reduce inflammatory reactions.

The villus-to-crypt ratio in the intestine, which is an important measure of gut health, showed an increase that was dependent on the pIgR dosage (Figs. S4(g) and (h) in Appendix A), suggesting that pIgR supported the repair of intestinal tissue damage caused by

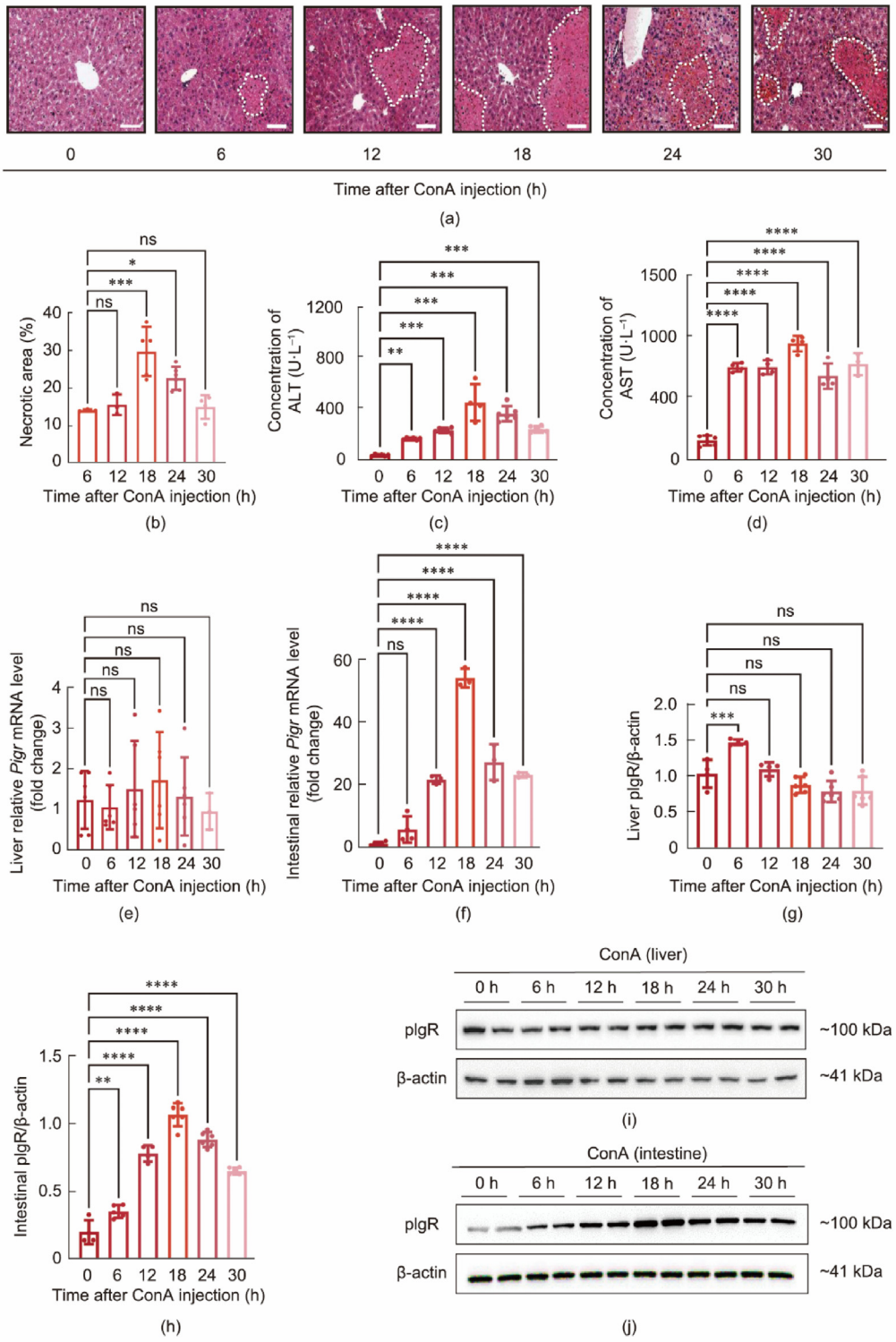

Fig. 2. Intestinal *Pigr* responsiveness to ConA-induced hepatic injury. (a) Representative H&E-stained section of liver (scale bar, 100 μm) and (b) measurements of necrotic area. (c) Serum ALT and (d) AST activity levels. Relative mRNA levels of (e) liver *Pigr* and (f) intestinal *Pigr* in mice. The ratios of (g) liver pIgR and (h) intestinal pIgR to total proteins. Equal amounts of lysates from (i) liver and (j) intestine were probed for pIgR (WB: pIgR). (b–h) $n = 6$ per group. Mean with standard deviation shown. One-way ANOVA. $^{*}P < 0.05$, $^{**}P < 0.01$, $^{***}P < 0.001$, $^{****}P < 0.0001$, ns: not significant.

ConA-induced hepatitis. Analysis of fecal samples by 16S ribosomal RNA sequencing demonstrated that the administration of pIgR caused a significant transformation in the composition of the intestinal microbiome. Principal coordinate analysis plots (Fig. S4(i) in Appendix A) demonstrated that the gut microbiota of mice treated with various doses of pIgR formed distinct clusters, indicating that community composition was influenced by the dose in a dose-dependent manner. However, all treatment groups showed significant divergence from the untreated ConA mice, indicating a general restorative effect of pIgR on the microbiota. As

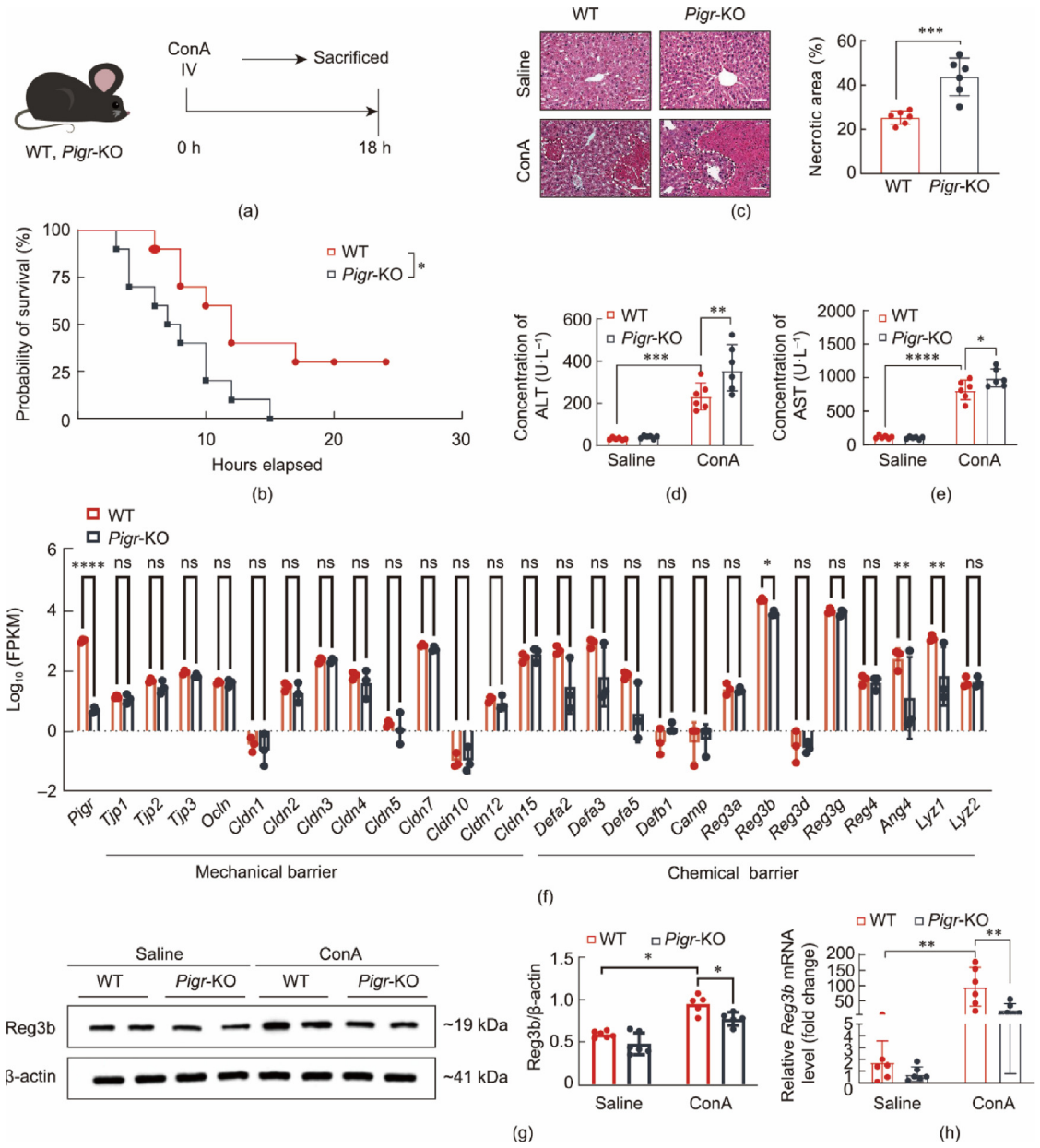

Fig. 3. Severe liver necrosis and reduced antimicrobial peptide secretion in *Pigr*-KO mice. (a) Schematic of ConA injection. (b) Survival curve of *Pigr*-KO mice and control mice (n = 10 per group). (c) Representative H&E-stained liver section (left; scale bar, 100 μm) and measurements of liver necrotic area (right). Serum levels of (d) ALT and (e) AST. (f) Changes in relative mRNA levels of genes related to intestinal physical barrier (*Tjp1–3*; *Ocln*; *Cldn1–5*, *7*, *10*, *12*, and *15*) and chemical barrier (*Defa2*, *3*, and *5*; *Defb1*; *Camp*; *Reg3a*, *3b*, *3d*, and *3g*; *Reg4*; *Ang4*; *Lyz1* and *2*) according to results of gene sequencing of gut tissue (n = 3 per group). (g) Equal amounts of lysates are probed for Reg3b (left) and their ratios to total proteins (right). (h) Relative mRNA levels of *Reg3b* in mice intestine. (c, f) Unpaired student t-test. (d, e, g, h) Two-way ANOVA. n = 6 per group. $^{*}P < 0.05$, $^{**}P < 0.01$, $^{***}P < 0.001$, $^{****}P < 0.0001$, ns: not significant; IV: intravenous injection; FPKM: fragments per kilobase of exon model per million mapped fragments.

shown in Fig. S4(j) in Appendix A, pIgR treatment exerted tailored modulation on specific taxa. *Akkermansia* were enriched by high-dose pIgR administration. Furthermore, the expression of Reg3b rose significantly in the intestinal tissues at both the mRNA and protein levels following pIgR administration (Figs. 4(f) and (h)). This result resembled the increase in Reg3b levels, suggesting that pIgR could potentially facilitate protective benefits by controlling the regulation of Reg3b.

Successful interference with the expression of Reg3b was achieved by injecting AAV9 into the tail vein, as demonstrated in Figs. S5(a) and (b) in Appendix A. Mice with reduced Reg3b expression displayed heightened intolerance to ConA, as evidenced by enhanced liver damage and elevated aminotransferase levels (Figs. S5(c)–(f) in Appendix A). In this particular instance, the administration of pIgR as a supplement did not relieve the liver immune damage induced by ConA. The expression of six inflammatory factors in the liver was analyzed (Figs. S5(g)–(l) in Appendix A). The main function of Reg3b was to exert its influence on pro-inflammatory factors, including *Il1β*, *Il17*, and *Tnfα*. In summary, we noted that pIgR could potentially safeguard the liver and facilitate gut healing, potentially through the augmentation of antimicrobial peptides, particularly Reg3b. The positive impacts of pIgR may aid in protecting the liver against hepatitis induced by ConA, potentially due to its hepatoprotective properties.

3.5. pIgR regulates Reg3b through the differentiation of innate lymphocytes promoted by IL-17D

Transcriptomic profiling of the intestinal mucosa of *Pigr*-KO AIH mice (Fig. 5(a)) revealed a notable reduction in the expression of

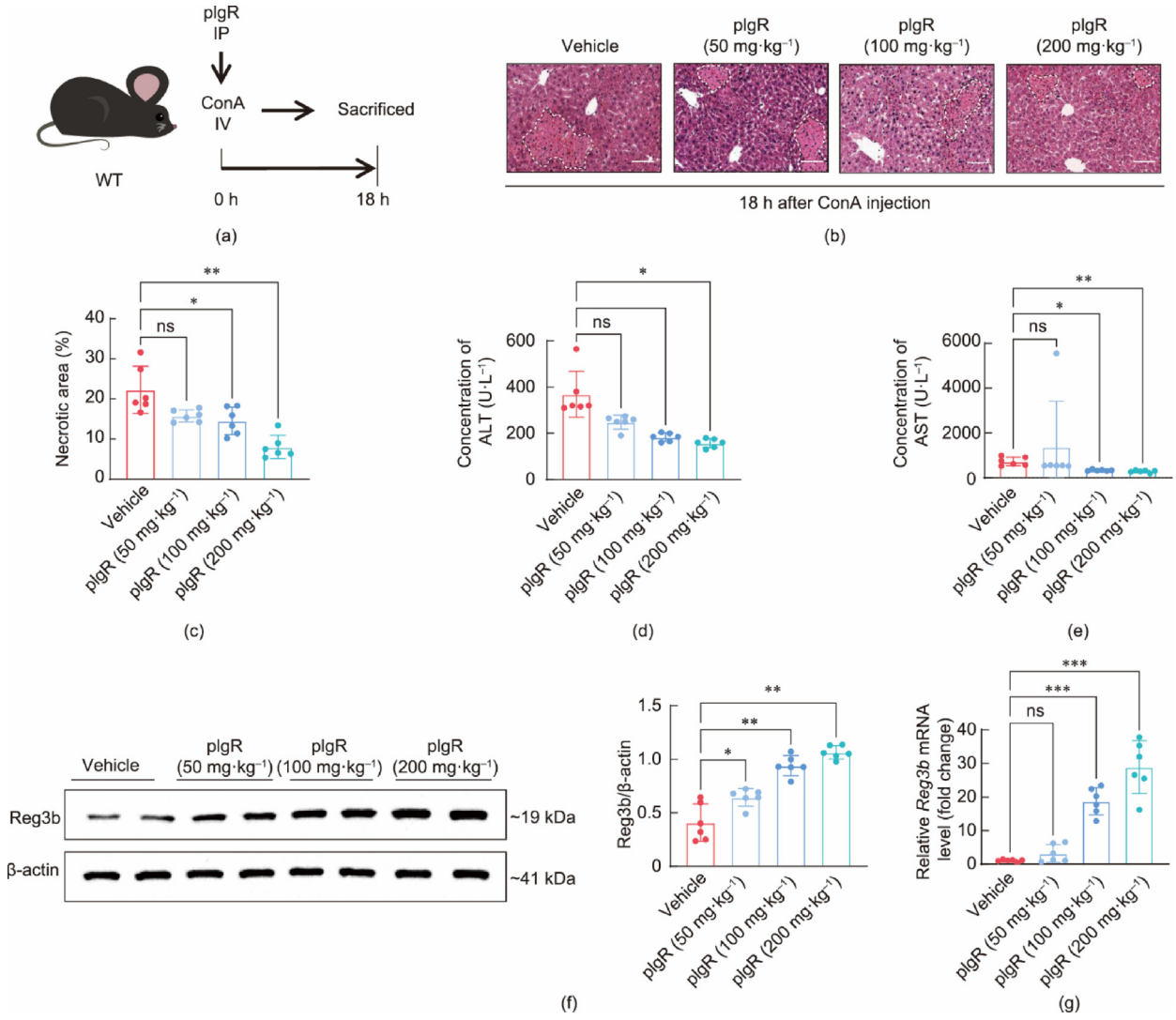

Fig. 4. Attenuated liver necrosis and increased antimicrobial peptide secretion in pIgR-treated mice. (a) Schematic of pIgR treatment regimen for AIH mice. (b) Representative H&E-stained section of liver (scale bar, 100 μm). (c) Measurements of necrotic area. Serum levels of (d) ALT and (e) AST. (f) Equal amounts of lysates are probed for Reg3b (left) and its ratios to total proteins (right). (g) Relative mRNA levels of *Reg3b* in mice intestine. (c–e, f, g) One-way ANOVA. $n = 6$ per group. $^{*}P < 0.05$, $^{**}P < 0.01$, $^{***}P < 0.001$, ns: not significant. IP: intraperitoneal injection.

genes related to Reg3b secretion. Key genes with decreased mRNA levels include *Mmp9*, *Il17d*, *Stat3*, and *Il17rd*, which play important roles in immune cell activation, Th17 responses, and maintenance of gut barrier function [25,26]. Co-repression of these factors may underlie gut dysbiosis and reduced Reg3b levels resulting from *Pigr* deficiency. According to Huang et al. [27], IL-17D activates group 3 innate lymphoid cells (ILC3s), thus boosting the production of the antimicrobial peptides, Reg3b and Reg3g. In *Pigr*-KO AIH mice, significant variations were observed in the downregulated expression of STAT3, IL-17D, and retinoic acid receptor alpha-related orphan receptor C (Rorc) (Figs. 5(b)–(f)). Conversely, AIH mice exhibited notable elevations in the levels of STAT3, IL-17D, and Rorc upon pIgR treatment at 200 mg·kg^{-1} (Figs. S6(a)–(e) in Appendix A). The natural cytotoxicity triggering receptor (NCR) and Rorc are biomarkers of ILC3s [28]. Flow cytometry was performed to investigate the activation of ILC3s by IL-17D in the regulatory mechanism of pIgR-controlled Reg3b secretion (Fig. 5(g)). Following *Pigr* knockout, the proportions of NCR^{+}ILC3 in the intestine of AIH mice decreased (Figs. 5(h)–(k)). Quantitative analysis showed that the production of IL-22 (Fig. 5(l)), a signature cytokine of intestinal NCR^{+}ILC3s [29], was markedly reduced in *Pigr*-KO mice. These data indicate that the genetic deficiency of pIgR results in quantitative impairment of ILC3 populations in the murine small intestine. However, the administration of the pIgR protein led to diametrically opposite effects. ELISA confirmed the increased production of IL-22 (Fig. S6(f) in Appendix A) and flow cytometry results showed an increased proportion of NCR^{+}ILC3 (Figs. S6(g)–(j) in Appendix A).

We administered IL-17D as a supplement to AIH mice (Fig. S7(a) in Appendix A). Both WT and *Pigr*-KO mice exhibited beneficial effects after IL-17D supplementation. Specifically, the administration of IL-17D as a supplement led to a reduction in the extent of liver necrosis, along with decreased levels of ALT and AST in *Pigr*-KO mice. Additionally, the levels of *Il1β*, *Ifnγ*, *Il17*, and *Tnfα* exhibited a decrease, whereas the levels of *Tgfβ* and *Il10* demonstrated an increase (Figs. S7(b)–(j) in Appendix A). We analyzed the expression of Reg3b in the intestinal tissues. Significant upregulation was observed in the expression of Reg3b in mice administered IL-17D solution compared to that in mice administered intraperitoneal saline injection (Figs. S7(k) and (l) in Appendix A). This phenomenon was also observed in mice lacking the *Pigr* gene. The effect of *Pigr* knockdown on AIH was partially mitigated by

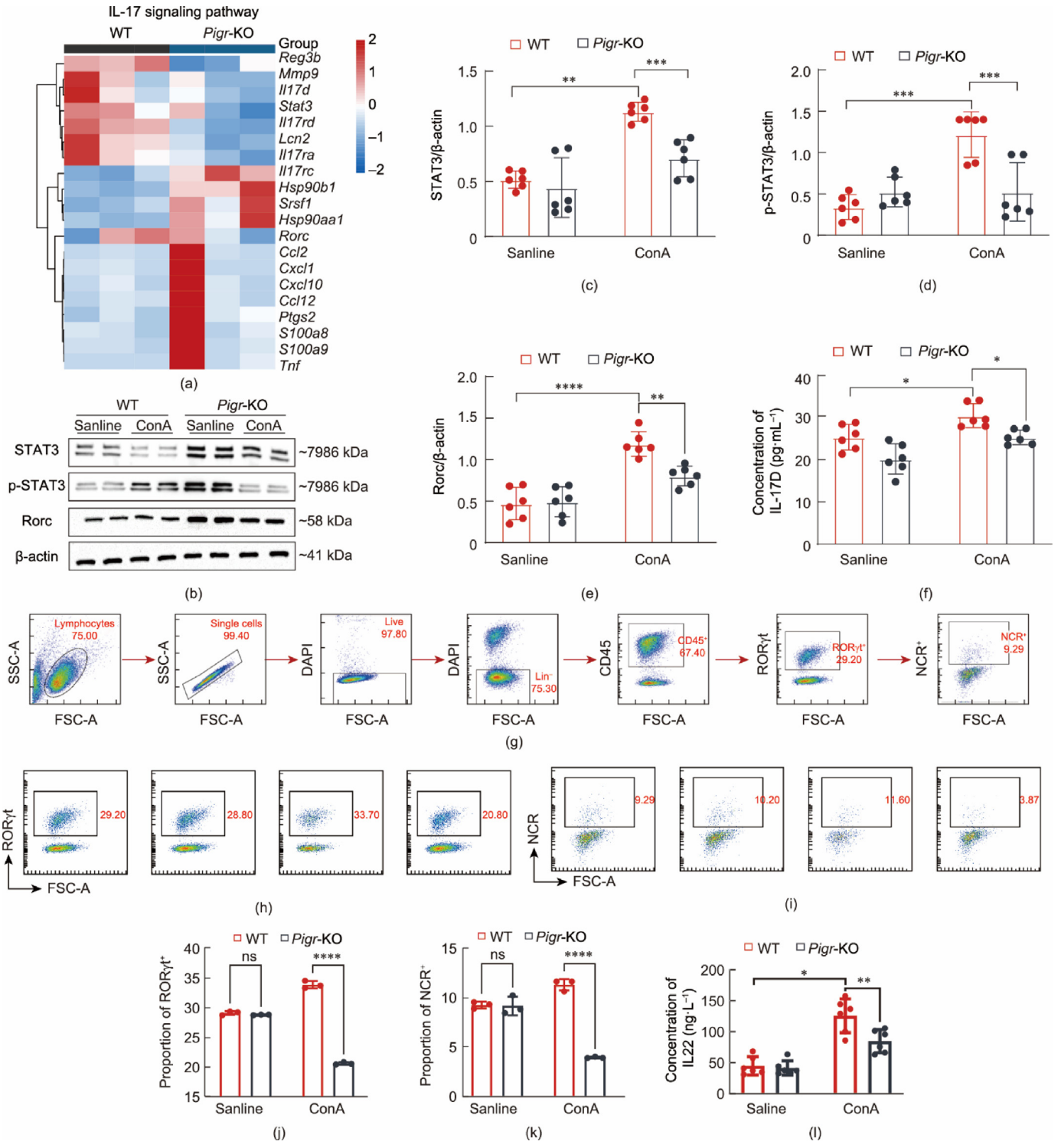

Fig. 5. Changes in the IL-17 pathway after *Pigr* knockout. (a) Heat map of differentially expressed genes in the IL-17 pathway ($n = 3$ per group). (b) Equal amounts of cell lysates are probed for STAT3, p-STAT3, and Rorc. Ratios of (c) STAT3, (d) p-STAT3, and (e) Rorc to total proteins. (f) ELISA for IL-17D. (g) Schematic representation of the cell flow gate. Flow cytometry to detect (h) RORγt and (i) NCR. Proportion of (j) RORγt$^+$ cells or (k) NCR$^+$ cells. (l) ELISA for IL-22. (c–f, l) $n = 6$ per group. Two-way ANOVA. (j, k) $n = 3$ per group. Two-way ANOVA. $^*P < 0.05$, $^{**}P < 0.01$, $^{***}P < 0.001$, $^{****}P < 0.0001$, ns: not significant. SSC-A: side scatter-A; FSC-A: forward scatter-A; LIN: lineage cocktail.

IL-17D supplementation. Additionally, supplementation with IL-17D significantly increased the proportion of NCR$^+$ILC3 (Figs. S7(m)–(p) in Appendix A).

In brief, our findings indicated that pIgR plays a role in controlling the secretion of Reg3b, partially by modulating IL-17D levels. The removal of *Pigr* in mice resulted in decreased IL-17D levels in the gut, along with reduced production of Reg3b. Supplementation with pIgR restored both IL-17D levels and Reg3b secretion. Taken together, these results suggest that pIgR exerts its effects on Reg3b, an antimicrobial peptide important for gut homeostasis, by increasing IL-17D production, most likely via ILC3s. Thus, the pIgR/IL-17D/Reg3b axis could serve as a vital pathway for preserving the well-being of the gastrointestinal tract and liver.

3.6. STAT3 plays an indispensable role in mediating the effects of pIgR on regulating IL-17 signaling and promoting ILC3 activation

We isolated primary small IECs and observed a significant decrease in the expression of both total STAT3 protein and phosphorylated STAT3 (p-STAT3) protein after *Pigr* knockout in ConA-induced mice (Figs. S7(q)–(s) in Appendix A). A reduction in the levels of both total STAT3 and p-STAT3 proteins induced by *Pigr* knockout was also evident in ConA models. To gain a deeper understanding of the function of STAT3 in controlling the healing properties of pIgRs in AIH, we infected the intestines of mice with AAV7 (Fig. 6(a)). The protective effects of pIgR against AIH were eliminated by interference with *Stat3*, as depicted in Figs. 6(b) and (c). Blockade of STAT3 signaling prevented pIgR from rescuing intestinal villous damage (Figs. 6(d) and (e)). Interception of STAT3 enhanced hepatic necrosis and subsequent pIgR supplementation failed to alleviate it, as indicated by the continuous increase in serum ALT and AST levels (Fig. 6(f) and (g)). Concurrently, Reg3b expression was markedly reduced following the STAT3 blockade (Figs. 6(h) and (i)). Effects of pIgR on IL-17 signaling and ILC3s activation were eliminated by inhibiting STAT3. After AAV7 administration, Rorc and IL-17D levels were notably reduced and were not restored by exogenous pIgR supplementation (Figs. 6(h), (j), (k)). Consistently, there were decreased proportions of NCR^+ and $ROR\gamma t^+$ cells, as well as reduced IL-22 production, observed in the intestinal LP cells of mice with blocked STAT3 signaling (Figs. 6(l)–(p)).

In summary, our results demonstrated that pIgR regulates IL-17-mediated inflammation and immunity, at least partly through STAT3-dependent mechanisms. Pharmacological blockade of STAT3 abrogated the ability of pIgR to stimulate ILC3 responses and alleviated AIH, suggesting that STAT3 serves as a critical node linking pIgR to the IL-17 signaling pathway.

3.7. pIgR protects the liver from LPS-induced damage

LPS, found in the outer membrane of Gram-negative bacteria, is the major bridge linking the gut and liver in the "gut–liver axis" [30]. After entering the bloodstream, LPS attaches to LPS-binding protein and CD14. This, in turn, activates Toll-like receptor 4 (TLR4) in immune cells and hepatocytes in the liver [31]. TLR4 stimulation leads to the activation of inflammatory signaling pathways and production of pro-inflammatory cytokines [32]. Compared to WT mice, *Pigr*-KO mice exhibited a substantial increase in serum LPS levels (Figs. 7(a)), whereas pIgR markedly decreased LPS levels in a dose-dependent manner (Fig. 7(b)), suggesting that pIgR negatively regulates LPS. Meanwhile, inhibition of STAT3 by AAV injection abrogated the effects of pIgR (Fig. 7(c)).

In *Pigr*-KO mice, TLR4 and myeloid differentiation factor 88 (MyD88), which are crucial for LPS signaling [33], exhibited higher expression (Figs. 7(d)–(f)). In AIH livers, pIgR treatment resulted in a dose-dependent decrease in TLR4 and MyD88 expression (Figs. 7(g)–(i)). Inhibition of STAT3 prevented the interaction between pIgR and LPS, potentially leading to the disruption of TLR4 and MyD88 attenuation (Figs. 7(j)–(l)).

By regulating the IL-17 pathway, expanding ILC3s, inducing antimicrobial peptides, and modulating gut microbiota composition, intestinal pIgR prevents LPS translocation from the gut to the liver to protect against AIH. Thus, pIgR functions as an important guardian through multipronged mechanisms that involve dampening of LPS signals via the TLR4/MyD88 axis in a STAT3-dependent manner.

4. Discussion

AIH, a liver disease characterized by chronic inflammation, is the result of an immune response that targets the liver tissue [34]. Inflammation and damage occur when the immune system erroneously targets liver cells. The exact causes remain unclear; however, genetic and environmental triggers may play a role in disrupting immune tolerance and initiating autoimmune responses [35]. Alterations in the microbiome as well as a "leaky gut" are associated with the immune system's state and the inflammatory response of the host [36]. However, whether these changes are disease-specific remains debatable [37]. In this investigation, we observed alterations in the gut microbiota of patients with AIH. *Bacteroides* and *Prevotella* produce LPS [20,38]. An elevated LPS load can promote inflammation and immune activation, contributing to the pathogenesis of AIH. *Blautia* and *Fecalibacterium* produce short-chain fatty acids (SCFAs) through fermentation [39,40]. Increased SCFAs may alter the gut barrier function and intestinal permeability, allowing bacterial antigens and endotoxins to leak into the blood and trigger autoimmune responses. *Akkermansia* and *Lactobacillus* are common probiotics that help maintain gut barrier integrity and modulate immune function [41]. These microbiota-induced disturbances could contribute to the initiation or worsening of AIH. Furthermore, the liver injury was aggravated after Abx treatment. This may be due to the disruption in the balance of gut microbes in WT mice, making the liver more susceptible to ConA stimulation [36]. The extent of liver injury was diminished in *Pigr*-KO mice that received antibiotic treatment, suggesting that the disruption of intestinal flora resulting from the knockdown of *Pigr* is a significant contributing factor to increased susceptibility to AIH.

Increased levels of pIgR exert multilayered beneficial effects on the intestine, helping to reduce liver injury in patients with AIH. The extracellular domain of pIgR facilitates binding of polymeric IgA and IgM, allowing their transport into the gut lumen and limiting bacterial translocation [42–44]. The absence of *Pigr* causes more severe intestinal damage, while the administration of varying doses of pIgR significantly improves gut morphology, suggesting that pIgR plays a role in preserving the integrity of the gut barrier. pIgR also increases the expression of antimicrobial peptides, such as Reg3b [45]. Reg3b can inhibit bacterial colonization and plays a role in regulating interactions between the microbiota and the immune system [9]. The protective effects of pIgR have been attributed to its antimicrobial activity.

The IL-17 signaling pathway is crucial for preserving the integrity of the intestinal barrier through the stimulation of mucus secretion and the production of antimicrobial peptides by epithelial cells [46,47]. In the intestine, IL-17 functions together with other cytokines, such as IL-22, to regulate immune responses [48]. The function of LC3s is regulated by IL-17D upon binding to CD93 [27]. However, IL-17 can also impair the gut barrier by inducing dysregulation of tight junction proteins and epithelial cell apoptosis [49]. This allows bacterial antigens and endotoxins to leak into the bloodstream, triggering an autoimmune response. IL-17 signaling has been shown to influence the composition of gut microbiota [50]. Elevated levels of IL-17 may partially mediate the dysbiosis associated with AIH. The role of pIgR in regulating ILC3s through IL-17D has been shown in this AIH model, suggesting that manipulating the IL-17 pathway by regulating pIgR could potentially control the severity of refractory AIH related to the intestinal tract and contribute to the maintenance of intestinal homeostasis.

After activation, STAT3 translocates to the nucleus and controls the expression of various genes related to immune cell differentiation [51]. Upon activation by cytokines or growth factors, STAT3 migrates to the nucleus and attaches to the *Il17* gene promoter [52,53]. This enhances the transcription of *Il17*, resulting in higher production of IL-17. IL-17 can attach to its receptor located on cells, leading to activation of the Janus kinase (JAK)-STAT pathway [54]. This process involves JAK enzymes that phosphorylate STAT3 pro-

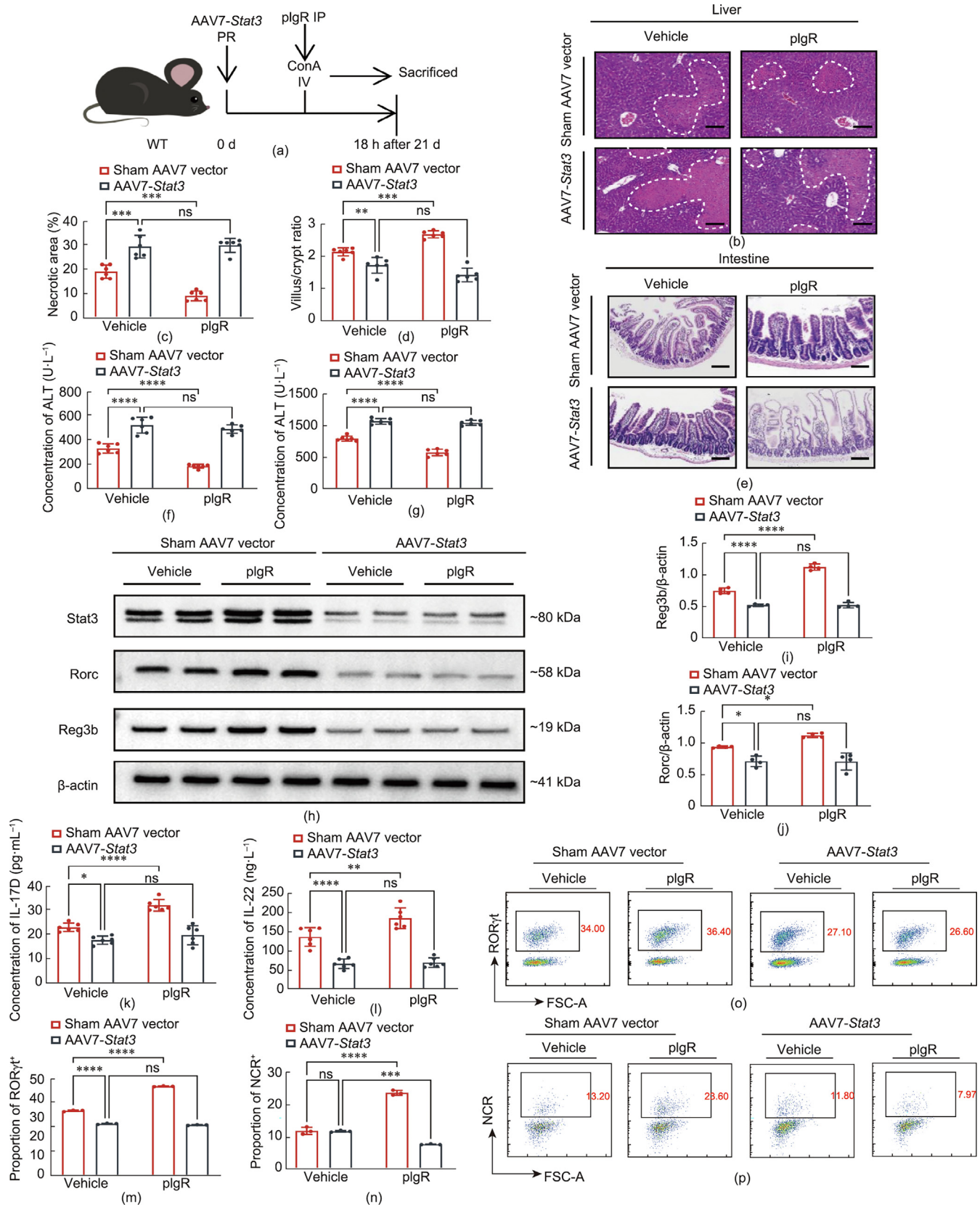

Fig. 6. Inhibition of STAT3 hinders the therapeutic effect of pIgR. (a) Schematic of the STAT3 inhibition regimen for pIgR-treated AIH mice. (b) Representative H&E-stained liver sections. (c) Measurement of necrotic areas (scale bar, 100 μm). (d) Measurements of V/C values. (e) Representative H&E-stained sections of the intestine (scale bar, 100 μm). Serum levels of (f) ALT and (g) AST levels. (h–j) Equal amounts of lysates are probed for Reg3b, Rorc, and their ratios to total proteins. ELISA for (k) IL-17D and (l) IL-22. Flow cytometry to detect (o) RORγt and (p) NCR. Proportion of (m) RORγt$^+$ cells or (n) NCR$^+$ cells. (c, d, f, i–l) $n = 6$ per group. Two-way ANOVA. (m, n) $n = 4$ per group. Two-way ANOVA. (m, n) $n = 3$ per group. Two-way ANOVA. $^*P < 0.05$, $^{**}P < 0.01$, $^{***}P < 0.001$, $^{****}P < 0.0001$, ns: not significant. PR: enema injection.

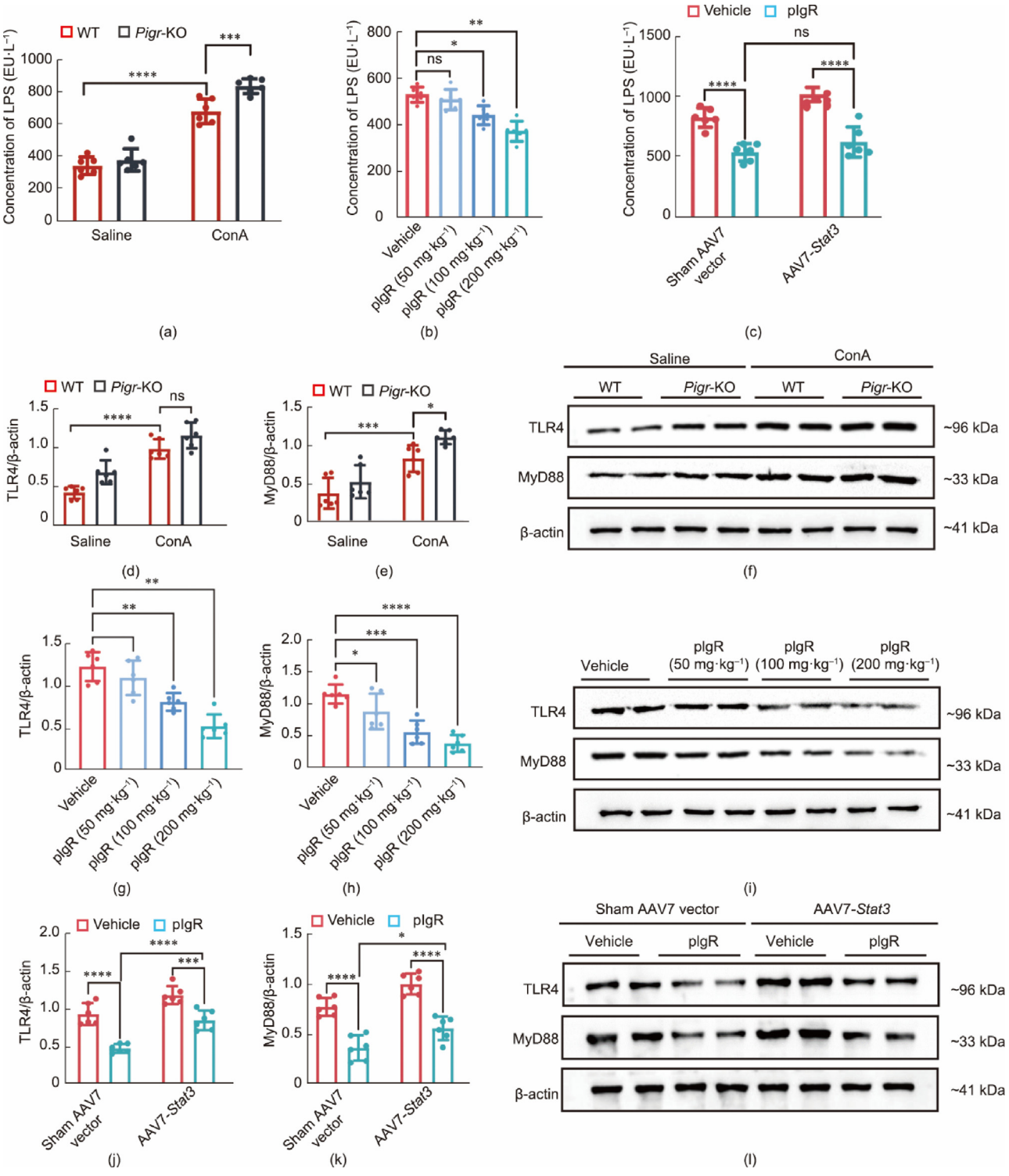

Fig. 7. pIgR protects the liver from LPS-induced damage. (a–c) Liver LPS activity levels. (d–f) Equal amounts of lysates are probed for TLR4 and MyD88 after *Pigr* knockout. (g–i) Equal amounts of lysates are probed for TLR4 and MyD88 after pIgR injection. (j–l) Equal amounts of lysates are probed for TLR4 and MyD88 after inhibition of STAT3. (a–c, e, f, h, i) $n = 6$ per group. (a, c, e, f, k, l) Two-way ANOVA. (b, h, i) One-way ANOVA. $^{*}P < 0.05$, $^{**}P < 0.01$, $^{***}P < 0.001$, $^{****}P < 0.0001$, ns: not significant. EU: endotoxin unit.

teins, which subsequently form dimers and move to the nucleus to regulate gene expression. This forms a positive feedback loop that amplifies Th17 differentiation and effector functions. The development of autoimmune conditions, such as rheumatoid arthritis and inflammatory bowel disease, is influenced by both STAT3 and IL-17 signaling. [55–57]. They appear to cooperate in driving chronic inflammation and tissue damage. Huang et al. [27] found that elimination of *Il17d* did not significantly modify *Stat3* levels, indicating that IL-17D may not operate primarily by activating STAT3 to regulate ILC3s. Our results showed that pharmacological inhibition of STAT3 activation could effectively eliminate the capacity of pIgR to stimulate the IL-17 pathway and ILC3s, suggesting that pIgR

functions, at least in part, via a STAT3-related mechanism. Overexpression of either pIgR or STAT3 increased IL-17D secretion.

Various nutritional interventions such as vitamins, probiotics, prebiotics, and specific dietary components have the potential to increase intestinal pIgR expression. The stimulation of murine secretory IgA and enhancement of pIgR transcripts have been demonstrated using chitosan oligosaccharides or polysaccharides from longan pulp [58,59]. Caloric restriction, an effective strategy for improving host physiology, also primes pIgR biosynthesis [60]. Vitamin A is an indispensable micronutrient that plays a pivotal role in the transcriptional regulation of pIgR [61]. The probiotic strain, *Saccharomyces cerevisiae boulardii* CNCM I-1079, potently modulated both pIgR expression and intestinal microbiota composition [62].

The present study had certain limitations. We observed a decrease in the abundance of *Akkermansia* in patient samples and mice with AIH, whereas an increase in *Akkermansia* abundance was observed in the *Pigr*-KO AIH models. This disparity could be attributed to variations in the microecological environment between human samples and animal models. In addition, the knockout of *Pigr* resulted in impairment of the intestinal barrier, thereby facilitating the proliferation of *Akkermansia*. Future studies should employ more comprehensive animal models to investigate the specific associations between pIgR and diverse intestinal bacteria. This will enhance the overall consistency and depth of scientific knowledge in this field. Further investigations are required to fully exploit the potential of the pIgR/STAT3/IL-17 pathway as a diagnostic indicator and therapeutic target for AIH. Overcoming existing constraints is crucial for effective utilization. Further longitudinal studies are required to validate specific microbiota profiles and gene expression levels as biomarkers of disease activity. Our study focused only on the pIgR/STAT3/IL-17 pathway and did not examine other signaling pathways that may be dysregulated in AIH. The interaction and crosstalk between the pIgR/STAT3/IL-17 pathway and other immune pathways remain unclear and require further investigation. Difficulties remain in the development of efficient and precise blockers with satisfactory safety records for extended periods of usage.

5. Conclusions

This study reveals that intestinal pIgR plays a crucial role in protecting against AIH by restricting the translocation of LPS from the intestine and modifying the balance of the immune system in the gut. Fundamental processes include the upregulation of IL-17D expression through the STAT3 signaling pathway, which is dependent on pIgR and partially regulates IL-17 signaling. This process activates ILC3s, enhances the production of antimicrobial peptides, and thus brings about changes in the composition of the gut microbiota. These combined effects ultimately restrict LPS production. Furthermore, intestinal pIgR negatively regulates liver inflammation by downregulating the LPS/TLR4/MyD88 signaling cascade. Collectively, our findings suggest that intestinal pIgR plays a pivotal role in protecting against AIH by restricting gut-derived LPS. Consequently, modulation of pIgR function could serve as a promising and innovative therapeutic approach for AIH.

Acknowledgments

This research was supported by the National Natural Science Foundation of China (82070593), the Zhejiang Provincial Natural Science Foundation (LD21H030002), the Department of Science and Technology of Zhejiang Province (ZY2019008), and the Young Scientists Fund of the National Natural Science Foundation of China (82200632). The authors would like to thank all the participants for their contributions.

Compliance with ethics guidelines

Ting Li, Tongtong Pan, Nannan Zheng, Xiong Ma, Xiaodong Wang, Fang Yan, Huimian Jiang, Yuxin Wang, Hongwei Lin, Jing Lin, Huadong Zhang, Jia Huang, Lingming Kong, Anmin Huang, Qingxiu Liu, Yongping Chen, and Dazhi Chen declare that they have no conflicts of interest or financial conflicts.

Appendix A. Supplementary data

Supplementary data to this article can be found online at https://doi.org/10.1016/j.eng.2024.01.006.

References

[1] Snijders RJALM, Assis DN, Oo YH, Sebode M, Taubert R, Willemse J, et al. Research gaps and opportunities in autoimmune hepatitis—results of the International Autoimmune Hepatitis Group Research Workshop 2022. Liver Int 2023;43(7):1375–84.
[2] Wang L, Cao ZM, Zhang LL, Li JM, Lv WL. The role of gut microbiota in some liver diseases: from an immunological perspective. Front Immunol 2022;13:923599.
[3] Liu Q, He W, Tang R, Ma X. Intestinal homeostasis in autoimmune liver diseases. Chin Med J 2022;135(14):1642–52.
[4] Kumar N, Arthur CP, Ciferri C, Matsumoto ML. Structure of the secretory immunoglobulin A core. Science 2020;367(6481):1008–14.
[5] Goguyer-Deschaumes R, Waeckel L, Killian M, Rochereau N, Paul S. Metabolites and secretory immunoglobulins: messengers and effectors of the host–microbiota intestinal equilibrium. Trends Immunol 2022;43(1):63–77.
[6] Simpfendorfer KR, Wang N, Tull DL, De Souza DP, Nahid A, Mu A, et al. Mus musculus deficient for secretory antibodies show delayed growth with an altered urinary metabolome. Mol Med 2019;25(1):12.
[7] Lin H, Lin J, Pan T, Li T, Jiang H, Fang Y, et al. Polymeric immunoglobulin receptor deficiency exacerbates autoimmune hepatitis by inducing intestinal dysbiosis and barrier dysfunction. Cell Death Dis 2023;14(1):68.
[8] Bluemel S, Wang L, Martino C, Lee S, Wang Y, Williams B, et al. The role of intestinal C-type regenerating islet derived-3 lectins for nonalcoholic steatohepatitis. Hepatol Commun 2018;2(4):393–406.
[9] Bajic D, Niemann A, Hillmer AK, Mejias-Luque R, Bluemel S, Docampo M, et al. Gut microbiota-derived propionate regulates the expression of Reg3 mucosal lectins and ameliorates experimental colitis in mice. J Crohns Colitis 2020;14(10):1462–72.
[10] Miki T, Holst O, Hardt WD. The bactericidal activity of the C-type lectin RegIIIβ against Gram-negative bacteria involves binding to lipid A. J Biol Chem 2012;287(41):34844–55.
[11] Standing D, Feess E, Kodiyalam S, Kuehn M, Hamel Z, Johnson J, et al. The role of STATs in ovarian cancer: exploring their potential for therapy. Cancers 2023;15(9):2485.
[12] Yue R, Wei X, Zhao J, Zhou Z, Zhong W. Essential role of IFN-γ in regulating gut antimicrobial peptides and microbiota to protect against alcohol-induced bacterial translocation and hepatic inflammation in mice. Front Physiol 2020;11:629141.
[13] Jin M, Zhang H, Wu M, Wang Z, Chen X, Guo M, et al. Colonic interleukin-22 protects intestinal mucosal barrier and microbiota abundance in severe acute pancreatitis. FASEB J 2022;36(3):e22174.
[14] Wang G, Tanaka A, Zhao H, Jia J, Ma X, Harada K, et al. The Asian Pacific Association for the study of the liver clinical practice guidance: the diagnosis and management of patients with autoimmune hepatitis. Hepatol Int 2021;15(2):223–57.
[15] Li J, Zhao F, Wang Y, Chen J, Tao J, Tian G, et al. Gut microbiota dysbiosis contributes to the development of hypertension. Microbiome 2017;5(1):14.
[16] He W, Wang ML, Jiang HQ, Steppan CM, Shin ME, Thurnheer MC, et al. Bacterial colonization leads to the colonic secretion of RELMbeta/FIZZ2, a novel goblet cell-specific protein. Gastroenterology 2003;125(5):1388–97.
[17] Walters W, Hyde ER, Berg-Lyons D, Ackermann G, Humphrey G, Parada A, et al. Improved bacterial 16S rRNA gene (V4 and V4–5) and fungal internal transcribed spacer marker gene primers for microbial community surveys. MSystems 2016;1(1):e00009–15.
[18] Elsherbiny NM, Rammadan M, Hassan EA, Ali ME, El-Rehim ASA, Abbas WA, et al. Autoimmune hepatitis: shifts in gut microbiota and metabolic pathways among Egyptian patients. Microorganisms 2020;8(7):1011.
[19] Wei Y, Li Y, Yan L, Sun C, Miao Q, Wang Q, et al. Alterations of gut microbiome in autoimmune hepatitis. Gut 2020;69(3):569–77.
[20] Lou J, Jiang Y, Rao B, Li A, Ding S, Yan H, et al. Fecal microbiomes distinguish patients with autoimmune hepatitis from healthy individuals. Front Cell Infect Microbiol 2020;10:342.

[21] Matsumura S, van de Water J, Leung P, Odin JA, Yamamoto K, Gores GJ, et al. Caspase induction by IgA antimitochondrial antibody: IgA-mediated biliary injury in primary biliary cirrhosis. Hepatology 2004;39(5):1415–22.
[22] Norderhaug IN, Johansen FE, Schjerven H, Brandtzaeg P. Regulation of the formation and external transport of secretory immunoglobulins. Crit Rev Immunol 1999;19(5–6):481–508.
[23] Hendrikx T, Lang S, Rajcic D, Wang Y, McArdle S, Kim K, et al. Hepatic pIgR-mediated secretion of IgA limits bacterial translocation and prevents ethanol-induced liver disease in mice. Gut 2023;72(10):1959–70.
[24] Chelakkot C, Ghim J, Ryu SH. Mechanisms regulating intestinal barrier integrity and its pathological implications. Exp Mol Med 2018;50(8):1–9.
[25] Mikami Y, Dobschütz EV, Sommer O, Wellner U, Unno M, Hopt U, et al. Matrix metalloproteinase-9 derived from polymorphonuclear neutrophils increases gut barrier dysfunction and bacterial translocation in rat severe acute pancreatitis. Surgery 2009;145(2):147–56.
[26] Damasceno LEA, Prado DS, Veras FP, Fonseca MM, Toller-Kawahisa JE, Rosa MH, et al. PKM2 promotes Th17 cell differentiation and autoimmune inflammation by fine-tuning STAT3 activation. J Exp Med 2020;217(10):e20190613.
[27] Huang J, Lee HY, Zhao X, Han J, Su Y, Sun Q, et al. Interleukin-17D regulates group 3 innate lymphoid cell function through its receptor CD93. Immunity 2021;54(4):673–86.
[28] Chan TY, Yen CL, Huang YF, Lo PC, Nigrovic PA, Cheng CY, et al. Increased ILC3s associated with higher levels of IL-1β aggravates inflammatory arthritis in mice lacking phagocytic NADPH oxidase. Eur J Immunol 2019;49(11):2063–73.
[29] Xie X, Zhao M, Huang S, Li P, Chen P, Luo X, et al. Luteolin alleviates ulcerative colitis by restoring the balance of NCR-ILC3/NCR$^+$ILC3 to repairing impaired intestinal barrier. Int Immunopharmacol 2022;112:109251.
[30] Zheng Z, Wang B. The gut–liver axis in health and disease: the role of gut microbiota-derived signals in liver injury and regeneration. Front Immunol 2021;12:775526.
[31] Ciesielska A, Matyjek M, Kwiatkowska K. TLR4 and CD14 trafficking and its influence on LPS-induced pro-inflammatory signaling. Cell Mol Life Sci 2021;78(4):1233–61.
[32] Chen SN, Tan Y, Xiao XC, Li Q, Wu Q, Peng YY, et al. Deletion of TLR4 attenuates lipopolysaccharide-induced acute liver injury by inhibiting inflammation and apoptosis. Acta Pharmacol Sin 2021;42(10):1610–9.
[33] Vatanen T, Kostic AD, d'Hennezel E, Siljander H, Franzosa EA, Yassour M, et al. Variation in microbiome LPS immunogenicity contributes to autoimmunity in humans. Cell 2016;165(4):842–53.
[34] Muratori L, Lohse AW, Lenzi M. Diagnosis and management of autoimmune hepatitis. BMJ 2023;380:e070201.
[35] Cardon A, Conchon S, Renand A. Mechanisms of autoimmune hepatitis. Curr Opin Gastroenterol 2021;37(2):79–85.
[36] Cheng Z, Yang L, Chu H. The gut microbiota: a novel player in autoimmune hepatitis. Front Cell Infect Microbiol 2022;12:947382.
[37] Goeser F, Münch P, Lesker TR, Lutz PL, Krämer B, Kaczmarek DJ, et al. Neither black nor white: do altered intestinal microbiota reflect chronic liver disease severity? Gut 2021;70(2):438–40.
[38] Jacobson AN, Choudhury BP, Fischbach MA. The biosynthesis of lipooligosaccharide from *Bacteroides thetaiotaomicron*. MBio 2018;9(2):e02289–10317.
[39] Wang B, Kong Q, Li X, Zhao J, Zhang H, Chen W, et al. A high-fat diet increases gut microbiota biodiversity and energy expenditure due to nutrient difference. Nutrients 2020;12(10):3197.
[40] Machiels K, Joossens M, Jo S, De Preter V, Arijs I, Eeckhaut V, et al. A decrease of the butyrate-producing species *Roseburia hominis* and *Faecalibacterium prausnitzii* defines dysbiosis in patients with ulcerative colitis. Gut 2014;63(8):1275–83.
[41] De Vos WM, Tilg H, Van Hul M, Cani PD. Gut microbiome and health: mechanistic insights. Gut 2022;71(5):1020–32.
[42] Zeng B, Wang H, Luo J, Xie M, Zhao Z, Chen X, et al. Porcine milk-derived small extracellular vesicles promote intestinal immunoglobulin production through pIgR. Animals 2021;11(6):1522.
[43] Matsumoto ML. Molecular mechanisms of multimeric assembly of IgM and IgA. Annu Rev Immunol 2022;40:221–47.
[44] Turula H, Wobus CE. The role of the polymeric immunoglobulin receptor and secretory immunoglobulins during mucosal infection and immunity. Viruses 2018;10(5):237.
[45] Reikvam DH, Derrien M, Islam R, Erofeev A, Grcic V, Sandvik A, et al. Epithelial–microbial crosstalk in polymeric Ig receptor deficient mice. Eur J Immunol 2012;42(11):2959–70.
[46] Schmitt H, Neurath MF, Atreya R. Role of the IL23/IL17 pathway in crohn's disease. Front Immunol 2021;12:622934.
[47] Willson TA, Jurickova I, Collins M, Denson LA. Deletion of intestinal epithelial cell STAT3 promotes T-lymphocyte STAT3 activation and chronic colitis following acute dextran sodium sulfate injury in mice. Inflamm Bowel Dis 2013;19(3):512–25.
[48] Geremia A, Arancibia-Cárcamo CV. Innate lymphoid cells in intestinal inflammation. Front Immunol 2017;8:1296.
[49] Lee JS, Tato CM, Joyce-Shaikh B, Gulen MF, Cayatte C, Chen Y, et al. Interleukin-23-independent IL-17 production regulates intestinal epithelial permeability. Immunity 2015;43(4):727–38.
[50] Dupraz L, Al M, Rolhion N, Richard ML, da Costa GG, Touch S, et al. Gut microbiota-derived short-chain fatty acids regulate IL-17 production by mouse and human intestinal γδ T cells. Cell Rep 2021;36(1):109332.
[51] Chun E, Lavoie S, Fonseca-Pereira D, Bae S, Michaud M, Hoveyda HR, et al. Metabolite-sensing receptor Ffar2 regulates colonic group 3 innate lymphoid cells and gut immunity. Immunity 2019;51(5):871–84.
[52] Zhao Y, Luan H, Jiang H, Xu Y, Wu X, Zhang Y, et al. Gegen Qinlian decoction relieved DSS-induced ulcerative colitis in mice by modulating Th17/Treg cell homeostasis via suppressing IL-6/JAK2/STAT3 signaling. Phytomedicine 2021;84:153519.
[53] Ernst M, Thiem S, Nguyen PM, Eissmann M, Putoczki TL. Epithelial gp130/Stat3 functions: an intestinal signaling node in health and disease. Semin Immunol 2014;26(1):29–37.
[54] Badr AM, Alkharashi LA, Sherif IO, Alanteet AA, Alotaibi HN, Mahran YF. IL-17/Notch1/STAT3 pathway contributes to 5-fluorouracil-induced intestinal mucositis in rats: amelioration by thymol treatment. Pharmaceuticals 2022;15(11):1412.
[55] Lee JY, Hall JA, Kroehling L, Wu L, Najar T, Nguyen HH, et al. Serum amyloid A proteins induce pathogenic Th17 cells and promote inflammatory disease. Cell 2020;180(1):79–91.e16.
[56] Ganesan R, Rasool M. Interleukin 17 regulates SHP-2 and IL-17RA/STAT-3 dependent Cyr 61, IL-23 and GM-CSF expression and RANKL mediated osteoclastogenesis by fibroblast-like synoviocytes in rheumatoid arthritis. Mol Immunol 2017;91:134–44.
[57] Lee SY, Lee SH, Yang EJ, Kim EK, Kim JK, Shin DY, et al. Metformin ameliorates inflammatory bowel disease by suppression of the STAT3 signaling pathway and regulation of the between Th17/Treg balance. PLoS One 2015;10(9):e0135858.
[58] Wen J, Niu X, Chen S, Chen Z, Wu S, Wang X, et al. Chitosan oligosaccharide improves the mucosal immunity of small intestine through activating SIgA production in mice: proteomic analysis. Int Immunopharmacol 2022;109:108826.
[59] Bai Y, Huang F, Zhang R, Ma Q, Dong L, Su D, et al. Longan pulp polysaccharide protects against cyclophosphamide-induced immunosuppression in mice by promoting intestinal secretory IgA synthesis. Food Funct 2020;11(3):2738–48.
[60] Lara-Padilla E, Campos-Rodríguez R, Jarillo-Luna A, Reyna-Garfias H, Rivera-Aguilar V, Miliar A, et al. Caloric restriction reduces IgA levels and modifies cytokine mRNA expression in mouse small intestine. J Nutr Biochem 2011;22(6):560–6.
[61] Sarkar J, Gangopadhyay NN, Moldoveanu Z, Mestecky J, Stephensen CB. Vitamin A is required for regulation of polymeric immunoglobulin receptor (pIgR) expression by interleukin-4 and interferon-gamma in a human intestinal epithelial cell line. J Nutr 1998;128(7):1063–9.
[62] Villot C, Chen Y, Pedgerachny K, Chaucheyras-Durand F, Chevaux E, Skidmore A, et al. Early supplementation of *Saccharomyces cerevisiae boulardii* CNCM I-1079 in newborn dairy calves increases IgA production in the intestine at 1 week of age. J Dairy Sci 2020;103(9):8615–28.